BMC Medical Imaging

RESEARCH

Open Access

Evaluation of deep learning-based reconstruction late gadolinium enhancement images for identifying patients with clinically unrecognized myocardial infarction

Xuefang Lu[1†], Weiyin Vivian Liu[2†], Yuchen Yan[1], Wenbing Yang[1], Changsheng Liu[1], Wei Gong[1], Guangnan Quan[3], Jiawei Jiang[4], Lei Yuan[5] and Yunfei Zha[1*]

Abstract

Background The presence of infarction in patients with unrecognized myocardial infarction (UMI) is a critical feature in predicting adverse cardiac events. This study aimed to compare the detection rate of UMI using conventional and deep learning reconstruction (DLR)-based late gadolinium enhancement (LGE_O and LGE_{DL}, respectively) and evaluate optimal quantification parameters to enhance diagnosis and management of suspected patients with UMI.

Methods This prospective study included 98 patients (68 men; mean age: 55.8 ± 8.1 years) with suspected UMI treated at our hospital from April 2022 to August 2023. LGE_O and LGE_{DL} images were obtained using conventional and commercially available inline DLR algorithms. The myocardial signal-to-noise ratio (SNR), contrast-to-noise ratio (CNR), and percentage of enhanced area (P_{area}) employing the signal threshold versus reference mean (STRM) approach, which correlates the signal intensity (SI) within areas of interest with the average SI of normal regions, were analyzed. Analysis was performed using the standard deviation (SD) threshold approach (2SD–5SD) and full width at half maximum (FWHM) method. The diagnostic efficacies based on LGE_{DL} and LGE_O images were calculated.

Results The SNR_{DL} and CNR_{DL} were two times better than the SNR_O and CNR_O, respectively ($P < 0.05$). $P_{area-DL}$ was elevated compared to P_{area-O} using the threshold methods ($P < 0.05$); however, no intergroup difference was found based on the FWHM method ($P > 0.05$). The $P_{area-DL}$ and P_{area-O} also differed except between the 2SD and 3SD and the 4SD/5SD and FWHM methods ($P < 0.05$). The receiver operating characteristic curve analysis revealed that each SD method exhibited good diagnostic efficacy for detecting UMI, with the $P_{area-DL}$ having the best diagnostic efficacy based on the 5SD method ($P < 0.05$). Overall, the LGE_{DL} images had better image quality. Strong diagnostic efficacy for UMI identification was achieved when the STRM was ≥ 4SD and ≥ 3SD for the LGE_{DL} and LGE_O, respectively.

†Xuefang Lu and Weiyin Vivian Liu contributed equally to this work.

*Correspondence:
Yunfei Zha
zhayunfei999@126.com

Full list of author information is available at the end of the article

Conclusions STRM selection for LGE_{DL} magnetic resonance images helps improve clinical decision-making in patients with UMI. This study underscored the importance of STRM selection for analyzing LGE_{DL} images to enhance diagnostic accuracy and clinical decision-making for patients with UMI, further providing better cardiovascular care.

Keywords Deep learning reconstruction, Diagnostic efficacy, Late gadolinium enhancement, Magnetic resonance imaging, Unrecognized myocardial infarction

Background

Myocardial infarction (MI) is diagnosed based on the detection of acute myocardial injury according to cardiac biomarker abnormalities in the context of acute myocardial ischemia [1]. Unrecognized MI (UMI) is a type of MI that has yet to be clinically diagnosed, with the prevalence increasing by 10.0% every decade [2]. Delayed detection due to atypical symptoms can delay treatment, leading to poor prognosis [3]. Failure to achieve reperfusion within a few hours after blood flow cessation may cause myocardial apoptosis in vessel-supplied regions. Therefore, determining the presence or absence of MI and quantifying related variables are crucial in improving the diagnosis, treatment, and prognosis [4, 5].

Cardiac magnetic resonance (CMR) imaging is a promising tool for MI detection because of good tissue contrast and spatial resolution. However, patient compliance is challenging for several reasons, such as the requirement to acquire each high-resolution slice and the need for stable respiration; furthermore, certain conditions, including unstable heartbeat and arrhythmia, can cause motion artifacts on free-breathing scans. As relatively shorter breath-holds are required to acquire more slices, higher-spatial resolution late gadolinium enhancement (LGE) is most frequently utilized in magnetic resonance imaging (MRI) to observe and quantify the degree of myocardial necrosis and microvascular occlusion. Although the enhancement is achieved semi-automatically using post-processing software, the initial sketch of the endocardium, epicardium, enhanced myocardium, and remote normal myocardium relies on the reader's experience to some extent [6]. Additionally, a previous study reported that LGE could identify only 23 of the 872 participants (2.6%) with UMI [7]. The clinical significance of UMI has been reported using different imaging techniques in diagnosing, refining risk stratification, and guiding clinical decisions for treatments. All underscored the role of CMR in improving the detection accuracy of UMIs, which may affect adverse cardiac outcomes and optimize cardiovascular disease management [8–10]. Therefore, timely and accurate UMI identification and assessment are fundamental for patient stratification and therapeutic planning [4, 5, 11]. In practice, despite many applications of standard deviation (SD) and full width at half maximum (FWHM) techniques, no consensus exists for quantifying scars on LGE images; this challenge persists across different cardiac diseases [12–14]. Obviously, a gap exists in current diagnostic frameworks for analyzing myocardium delayed enhancement.

Deep learning (DL) methods can improve image quality and eliminate intra- and inter-observer variability, enabling more accurate diagnosis and treatment strategies [15, 16] and segmentation for precisely sketched lesions [17–21], among others. However, no DL reconstruction (DLR)-based magnetic resonance (MR) studies have evaluated patients with suspected UMI. Therefore, this study aimed to explore the feasibility and diagnostic performance of DLR-based LGE imaging (LGE_{DL}) for patients with UMI compared with that of conventional imaging (LGE_{O}) and propose an appropriate signal threshold versus reference mean (STRM) for analyzing LGE_{DL}.

Methods

Study population

This study prospectively recruited 98 patients (68 men and 30 women, mean age: 55.8±8.1 years) who presented at our hospital between April 2022 and August 2023 without typical MI symptoms, such as angina pectoris of cardiogenic origin but with suspected UMI after a physical examination. Based on the guidelines of European and American associations and previous reports [1, 7, 22], the inclusion criteria were as follows: (i) the absence of typical angina symptoms; (ii) the presence of elevated or decreased serum cardiac troponin (cTn) levels, with at least one instance of elevation above the upper limit of the normal value (the 99th percentile of the reference value's upper limit); (iii) prior evidence of MI on electrocardiography in the absence of left ventricular hypertrophy and left bundle branch block; and (iv) no prior history of oncological disease or surgery for cardiovascular diseases. The exclusion criteria were as follows: (i) clinically unstable condition, decompensated heart failure, contraindication to CMR, an estimated glomerular filtration rate≤30 mL/min, and contraindication to the use of gadolinium contrast; and (ii) LGE images that could not be used for clinical diagnosis and objective assessments (Fig. 1).

CMR examination and image construction

All patients underwent a routine cardiac MRI examination, including a short-axis LGE imaging sequence, on a 3.0-T MRI scanner (Signa Architect, GE Healthcare, Waukesha, WI, USA) at our hospital. A new

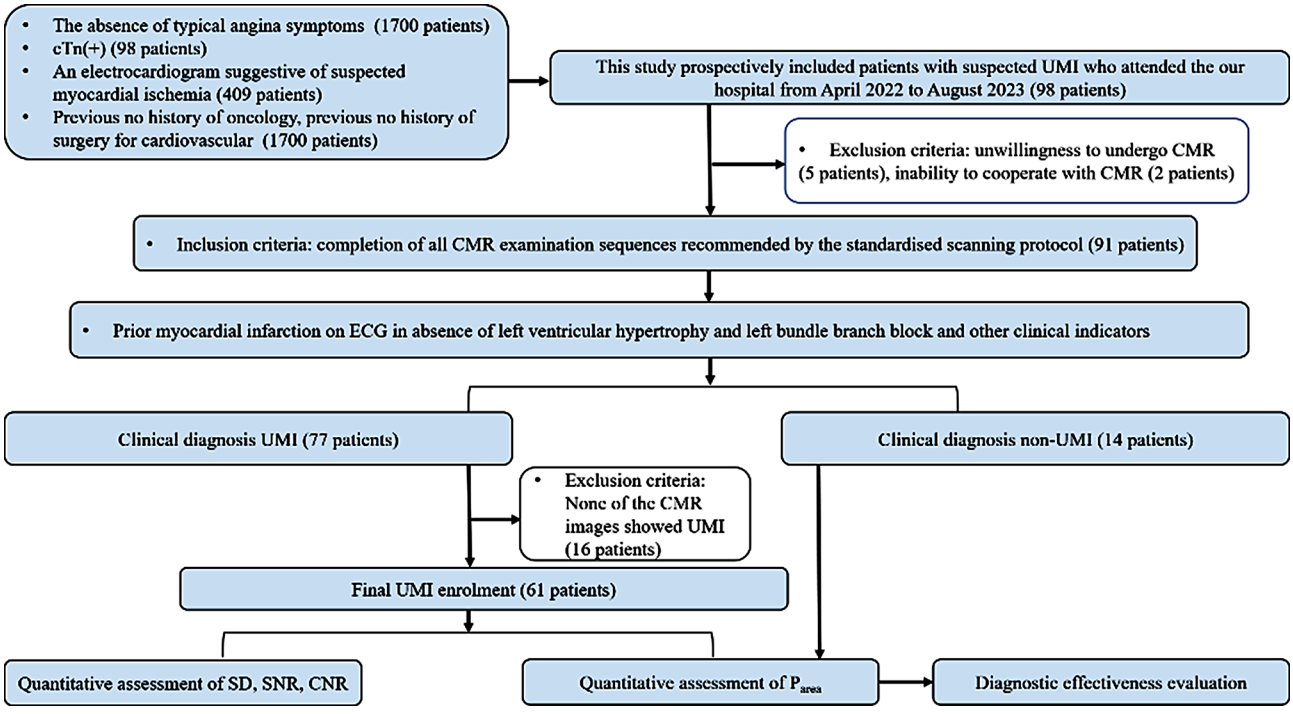

Fig. 1 Flowchart of patient enrolment and exclusion. Note: cTn: cardiac troponin; ECG: electrocardiogram; LGE_O: conventionally constructed late gadolinium enhancement; LGE_{DL}: deep learning-based reconstruction late gadolinium enhancement; UMI: unrecognized myocardial infarction; SD: standard deviation; SNR: signal-to-noise ratio; CNR: contrast-to-noise ratio

commercial inline deep-learning-based reconstruction (DLR, brand name: AIR™ Recon DL, DV29.1_R04, GE Healthcare, USA) employs no bias terms and rectified linear unit activations to identify 4.4 million features on directly received image data immediately after scanning on an MR console computer to reduce noise and Gibbs artifacts, and further eliminate intra- and inter-observer differences [13, 16]. The parameters for the LGE sequence were as follows: echo time=2.7 ms; repetition time=5.6 ms; flip angle=25°; field of view=34 mm; matrix=260×174; slice thickness=8 mm; slice spacing=2 mm; receiver bandwidth=83.33 kHz; views per segment=24; number of excitations=1; and theoretical acquisition time=8 s×nine heart beats. The LGE_O and LGE_{DL} were simultaneously generated using conventional inline reconstruction and AIR™ Recon DL algorithms. Fifteen minutes before LGE sequence scanning, a single bolus of 0.1 mmol/kg (0.2 ml/kg) Gadobenate Dimeglumine (Bracco Imaging S.P.A., Milano, Italy) was administered, followed by 20-mL saline flush at a flow rate of 2 ml/s [23]. This dosage was selected based on its efficacy of myocardial enhancement for visualization under the condition of patient safety.

Assessment of myocardial enhancement area and diagnostic efficacy

Ultimately, data from 61 patients with myocardial enhancement were included in the analysis (43 men [70.5%] and 18 women [29.5%]), with a mean age of 55.9±8.7 years (Fig. 1). The percentage of whole-heart myocardial enhancement area (P_{area}) in segments S1–S16 was assessed semi-quantitatively to diagnose cardiovascular disease using Circle Cardiovascular Imaging Inc. (cvi[42], Circle Cardiovascular Imaging Inc., Calgary, AB, Canada). The delayed enhancement area (i.e., scar size) was subsequently quantified based on threshold methods, which involve adding 2–5 times SD to the mean signal intensity (SI) of the reference myocardium, and the FWHM method, which identifies the half maximum SI at the full width of SI distribution within one region of interest (ROI) in the myocardial tissue. The P_{area} was calculated as the scar size divided by the myocardial volume. Furthermore, the diagnostic efficacy of the P_{area} of LGE_{DL} and LGE_O images ($P_{area-DL}$ and P_{area-O}, respectively) in differentiating patients with UMI was assessed, with the clinical diagnosis of UMI as the gold standard.

Theory/calculation

CMR image assessment

Qualitative and quantitative imaging evaluations were performed double-blindedly by two radiologists with >5 years of experience in CMR diagnosis. Moreover, one of the radiologists repeated the assessment 1 month later.

Image quality

For the objective evaluation of image quality, ROIs were on LGE_O and LGE_{DL} images to determine the SI of the normal myocardium (SI_{Myo-O} and SI_{Myo-DL}, respectively) and myocardial delayed enhancement area (SI_{MDEA-O} and $SI_{MDEA-DL}$, respectively), as well as the SD of the background noise at the corner of the images (SD_{BG-O} and SD_{BG-DL}, respectively) and the myocardial delayed enhancement area (SD_{MDEA-O} and $SD_{MDEA-DL}$, respectively) (Fig. 2). Additionally, for LGE_O and LGE_{DL} images, the myocardial signal-to-noise ratios (SNRs) (SNR_O and SNR_{DL}, respectively) and contrast-to-noise ratios (CNRs) (CNR_O and CNR_{DL}, respectively) were calculated [9, 10, 24, 25] using the following formulae:

$$SNR = SI_{Myo}/SD_{BG}$$

$$CNR = |SI_{MDEA} - SI_{Myo}|/(1.5SD_{BG})$$

The short-axis LGE_O and LGE_{DL} images were divided into 16 segments based on the American Heart Association criteria, and the SNR and CNR of each segment were calculated.

Statistical analysis

All data were statistically analyzed using R-project software (version 4.0.4, http://www.r-project.org). Quantitative data are expressed as either the $\bar{x} \pm SD$ or median (interquartile range). All quantitative data were analyzed using either a paired *t*-test or a Wilcoxon signed-rank test depending on the results of the Shapiro–Wilk and Levene's tests, which were used to assess variance homogeneity and data normality, respectively. To control the false discovery rate, we applied the Benjamini–-Hochberg method for multiple comparison corrections. The intraclass correlation coefficients (ICCs) of the objective quantitative indicators, including the SNR, CNR, SD, and P_{area} for LGE_O and LGE_{DL} images (SNR_O, SNR_{DL}, CNR_O, CNR_{DL}, SD_O, SD_{DL}, P_{area-O} and $P_{area-DL}$, respectively) were quantified to assess the degree of intra- and inter-observer agreement. Receiver operating characteristic (ROC) curves for $P_{area-DL}$ and P_{area-O} were constructed using the different threshold methods to determine and compare their diagnostic efficacies for the UMI or non-UMI groups based on the area under the curve (AUC). All statistical significance was set at $P<0.05$.

Results

Patient characteristics

Overall, 77 patients (53 men and 24 women; mean age: 55.6±8.4 years) were diagnosed with UMI based on various clinical indicators, including the cTn level ($n=77$), imaging features on electrocardiography ($n=77$), ultrasound cardiography ($n=18$), computed tomography angiography ($n=14$), and digital subtraction angiography ($n=38$), or nuclear medicine test results ($n=8$). Sixty-one patients (43 men and 18 women; mean age: 55.9±8.7 years) who met the UMI diagnostic criteria were evaluated to assess the distribution of the supplying vessels

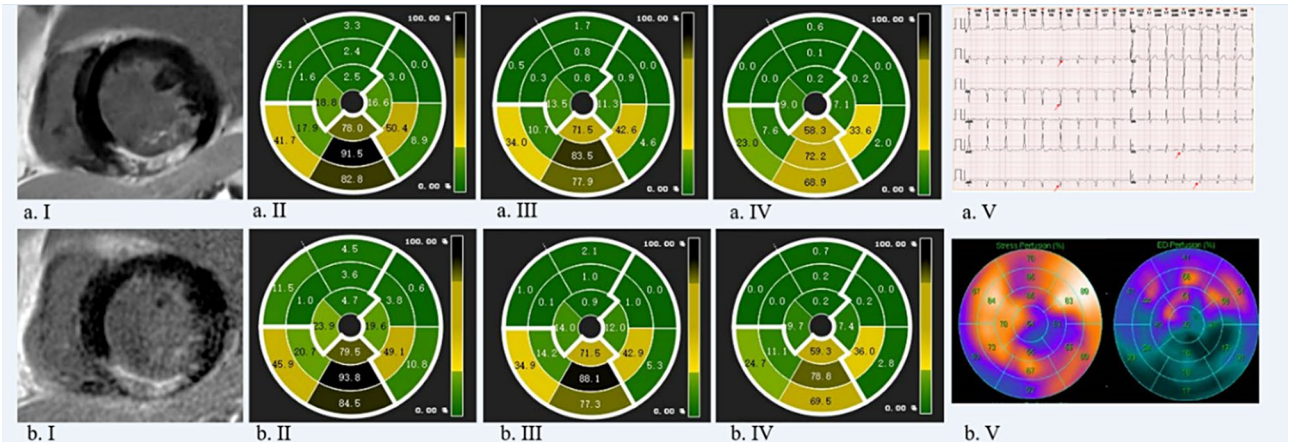

Fig. 2 Schematic diagram of P_{area} using accordingly (a.II) and (b.III) 4SD, (b.II) 3SD, (a.III) 5SD, (a.IV) and (b.IV) FWHM methods for (a) LGE_{DL} images, (b) LGE_O images, and (a. V) electrocardiogram of a patient with UMI. Figure 2(a) shows clearer, less noisy, more uniform normal myocardial signal and better contrast between the enhancement area and normal myocardium than Fig. 2(b). The patient with UMI underwent stress perfusion myocardium and received an intravenous injection of 20 mCi 99mTc-MIBI. The stress perfusion maps as Fig. 2(b. V) supported our P_{area} maps with clearer myocardium enhancement in the enlarged left ventricle, with the morphological anomaly, relatively light sparsity of 20 mCi 99mTc-MIBI (a radiation tracker, RT) in the middle and basal segments of the anterior wall and the middle segment of the anteroseptal wall, relatively strong sparsity of RTs in the apex, the apical segment of the septal wall, the middle and basal segments of the posteroseptal wall, the apical, middle, and basal segments of the inferior wall, the apical segment of the lateral wall, and the middle and basal segments of posterolateral, and normal perfusion in the remaining myocardium. Note: SD: standard deviation; 2, 3, 4, and 5SD threshold methods: mean P_{area} respectively adding 2, 3, 4, and 5 times of standard deviation of P_{area} as the threshold for myocardial enhancement area; FWHM: full width at half maximum; LGE_{DL}: deep learning-based reconstruction late gadolinium enhancement; LGE_O: conventionally constructed late gadolinium enhancement; UMI: unrecognized myocardial infarction

and the presence of infarction in LGE images. The non-UMI group predominantly exhibited hypertrophic cardiomyopathy ($n=10$, 71.43%) and left bundle branch block ($n=4$, 28.57%) (Fig. 1).

Objective evaluation of image quality

The SDs of the normal myocardium, delayed myocardial enhancement areas, and background of the images are presented in Table 1. The SD_{DL} values were lower than the SD_O values in all 16 segments, with the S1 segment exhibiting the most significant difference between SD_{DL} and SD_O images (31.95±21.82 vs. 45.74±28.29, $P<0.05$). Overall, the SD_{Myo-DL}, $SD_{MDEA-DL}$, and SD_{BG-DL} values of LGE_{DL} images were lower than the respective values of LGE_O images, including the SD_{Myo-O} (36.38±19.55 vs. 46.03±18.65, $P<0.05$), SD_{MDEA-O} (47.39±41.22 vs. 59.77±44.08, $P<0.05$), and SD_{BG-O} (3.14±2.48 vs. 6.17±4.03, $P<0.05$). The SNR_{DL} values were higher than the SNR_O values in all 16 segments ($P<0.001$), with the most significant difference observed in the S16 segment (92.44±78.39 vs. 27.39±24.56, respectively; $P<0.05$). The S1 segment exhibited the highest SNR_{DL} (113.89±98.62), and the S2 segment had the highest SNR_O (39.10±41.45). The whole myocardial SNR_{DL} and whole delayed myocardial enhancement CNR_{DL} were significantly elevated compared to the whole myocardial SNR_O (99.93±81.42 vs. 33.29±30.89, $P<0.05$) and whole delayed enhanced myocardium CNR_O (123.72±45.00 vs. 60.15±15.52, $P<0.05$), respectively (Fig. 2a-b–.I, Supplementary Fig. 1a–d.I). The SI_{DL} values were higher than the respective SI_O values for all segments ($P<0.05$) except for S7–S9 and S11. In comparing the SI_{Myo-DL} and SI_{Myo-O} values, the SI_{DL} values were higher than the corresponding SI_O values for S1–S6, S10, and S12–S16 ($P<0.05$). The SI_{DL} values were slightly higher than the corresponding SI_O values for S7–S9 or S11; however, the difference was not significant ($P>0.05$) (Fig. 3a).

P_{area} assessment

The myocardial enhancement area was semi-quantitatively analyzed using various SD thresholds and the FWHM method. For the 2SD (Fig. 3b.**I, Supplementary Figs. 1**), 3SD (Figs. 2 and 3b.II, Supplementary Fig. 1), and 5D methods (Figs. 2 and 3b.IV, Supplementary Fig. 1), the $P_{area-DL}$ values for the overall myocardium were higher than the corresponding P_{area-O} values for all 16 segments. For the 4SD method, the $P_{area-DL}$ values of the overall myocardium were higher than the corresponding P_{area-O} values only in S1–S12 (Figs. 2 and 3b.III, Supplementary Fig. 1). For the FWHM method (Figs. 2 and 3.c, Supplementary Fig. 1), the $P_{area-DL}$ values were slightly higher than the corresponding P_{area-O} values for all segments.

Regarding the DLR-based P_{area}, the overall different threshold and FWHM-based $P_{area-DL}$ values were higher than those based on any other approach (all $P<0.05$). Regarding the P_{area-O}, the values for the 2SD threshold were significantly higher than those based on other approaches (all $P<0.05$) (Table 2).

Table 1 Objective evaluation of image quality for LGE_{DL} and LGE_O

	SD				SNR			
	LGE_{DL}	LGE_O	t/Z	p	LGE_{DL}	LGE_O	t/Z	p
S1	31.95±21.82	45.74±28.29	5.592	< 0.05	113.89±98.62	33.58±33.36	4.759	< 0.05
S2	36.04±28.27	47.19±30.01	4.522	< 0.05	106.97±103.87	39.10±41.45	3.724	< 0.05
S3	43.34±30.63	52.37±26.63	3.272	< 0.05	98.82±93.38	38.16±41.42	3.667	< 0.05
S4	33.05±20.62	49.28±23.02	5.498	< 0.05	91.24±85.00	32.62±34.86	4.033	< 0.05
S5	39.44±21.07	54.61±24.43	5.111	< 0.05	103.87±98.09	38.78±39.78	3.767	< 0.05
S6	32.77±16.73	45.97±23.14	5.014	< 0.05	94.96±85.96	33.38±36.85	4.105	< 0.05
S7	34.42±27.18	40.79±22.09	2.521	< 0.05	100.95±86.57	32.86±30.23	4.83	< 0.05
S8	30.44±26.95	44.75±39.61	4.877	< 0.05	105.97±94.58	33.87±33.44	4.493	< 0.05
S9	36.21±29.37	45.13±29.37	4.374	< 0.05	96.92±86.47	34.78±37.62	4.155	< 0.05
S10	37.10±27.54	47.98±29.08	4.647	< 0.05	104.39±90.32	34.46±35.53	4.399	< 0.05
S11	40.92±32.34	49.84±32.27	3.390	< 0.05	98.00±88.76	35.03±34.21	4.241	< 0.05
S12	40.24±22.70	45.43±21.20	2.704	< 0.05	97.53±85.58	30.49±32.78	4.845	< 0.05
S13	28.45±18.92	38.97±21.52	4.845	< 0.05	102.41±91.98	33.74±33.13	4.522	< 0.05
S14	31.75±22.24	40.39±24.62	5.046	< 0.05	82.85±80.32	24.64±27.49	4.371	< 0.05
S15	33.68±21.04	43.25±24.02	3.081	< 0.05	107.57±95.83	29.81±29.20	4.866	< 0.05
S16	36.33±22.36	44.71±25.96	2.956	< 0.05	92.44±78.39	27.39±24.56	5.039	< 0.05
WM	36.38±19.55	46.03±18.65	5.789	< 0.05	99.93±81.42	33.29±30.89	4.644	< 0.05
MDEA	47.39±41.22	59.77±44.08	6.206	< 0.05				
BG	3.14±2.48	6.17±4.03	6.052	< 0.05				

Note: SD, standard deviation; SNR, signal-to-noise ratio; WM, whole myocardium; MDEA, myocardium delayed enhancement area; BG, background

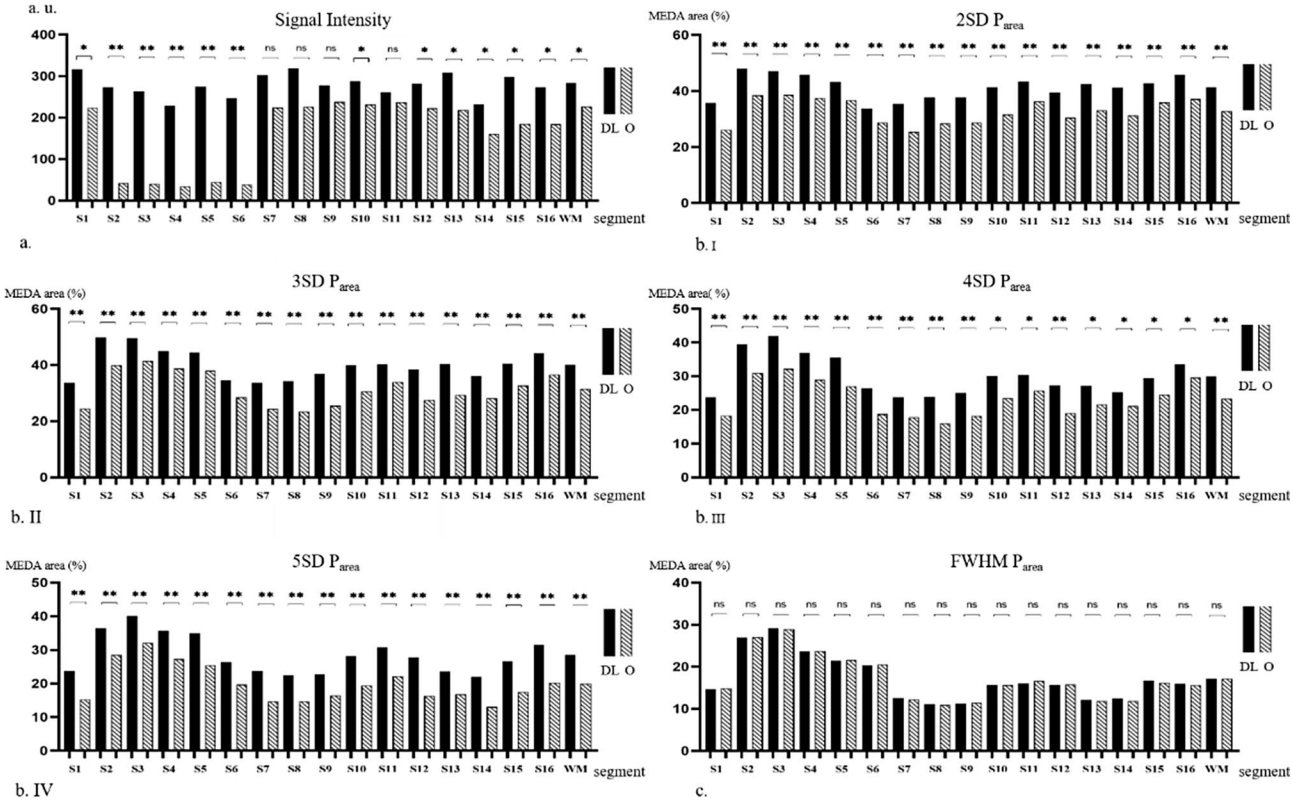

Fig. 3 (a) Signal intensity of the left ventricular myocardial on LGE_{DL} and LGE_{O} images. Percentage areas of left ventricular myocardial enhancement in LGE_{DL} and LGE_{O} images using (b. I) 2SD, (b. II) 3SD, (b. III) 4SD, (b. IV) 5SD, and (c) FWHM methods for quantification. Note: SI: signal intensity; WM: whole myocardium; P_{area}: percentage of myocardial enhancement area; LGE_{DL}: deep learning-based reconstruction late gadolinium enhancement; LGE_{O}: conventionally constructed late gadolinium enhancement;; SD: standard deviation; 2, 3, 4, and 5SD threshold methods: mean P_{area} respectively adding 2, 3, 4, and 5 times of standard deviation of P_{area} as the threshold for myocardial enhancement area; FWHM: full width at half maximum; DL, deep learning late gadolinium enhancement; O: original late gadolinium enhancement

Table 2 Differences between different-threshold and FWHM methods

	LGE_{DL}			LGE_{O}		
		t	*p*		t	*p*
2SD P_{area} vs. 3SD P_{area}	41.32 ± 12.78 vs. 39.83 ± 16.58	1.454	>0.05	32.81 ± 12.59 vs. 31.41 ± 16.07	1.808	>0.05
2SD P_{area} vs. 4SD P_{area}	41.32 ± 12.78 vs. 30.57 ± 15.25	8.390	< 0.05	32.81 ± 12.59 vs. 23.96 ± 12.79	7.644	< 0.05
2SD P_{area} vs. 5SD P_{area}	41.32 ± 12.78 vs. 28.53 ± 12.92	12.072	< 0.05	32.81 ± 12.59 vs. 19.98 ± 12.73	11.836	< 0.05
2SD P_{area} vs. FWHM P_{area}	41.32 ± 12.78 vs. 17.25 ± 11.22	10.567	< 0.05	32.81 ± 12.59 vs. 17.18 ± 11.12	7.375	< 0.05
3SD P_{area} vs. 4SD P_{area}	39.83 ± 16.58 vs. 30.57 ± 15.25	10.342	< 0.05	31.41 ± 16.07 vs. 23.96 ± 12.79	7.468	< 0.05
3SD P_{area} vs. 5SD P_{area}	39.83 ± 16.58 vs. 28.53 ± 12.92	10.963	< 0.05	31.41 ± 16.07 vs. 19.98 ± 12.73	14.059	< 0.05
3SD P_{area} vs. FWHM P_{area}	39.83 ± 16.58 vs. 17.25 ± 11.22	8.878	< 0.05	31.41 ± 16.07 vs. 17.18 ± 11.12	5.695	< 0.05
4SD P_{area} vs. 5SD P_{area}	30.57 ± 15.25 vs. 28.53 ± 12.92	2.142	< 0.05	23.96 ± 12.79 vs. 19.98 ± 12.73	5.474	< 0.05
4SD P_{area} vs. FWHM P_{area}	30.57 ± 15.25 vs. 17.25 ± 11.22	5.733	< 0.05	23.96 ± 12.79 vs. 17.18 ± 11.12	3.048	< 0.05
5SD P_{area} vs. FWHM P_{area}	28.53 ± 12.92 vs. 17.25 ± 11.22	4.964	< 0.05	19.98 ± 12.73 vs. 17.18 ± 11.12	1.314	>0.05

Note: LGE_{DL}, deep learning-based reconstruction late gadolinium enhancement; LGE_{O}, conventionally constructed late gadolinium enhancement; P_{area}, percentage of myocardial enhancement area; FWHM, full width at half maximum

Assessment of the consistency of the quantitative measurements

The degree of intra- and inter-observer agreement for the objective measurements (SD_{Myo}, SD_{MDEA}, SD_{BG}, SNR, CNR, and SI_{Myo}) and P_{area} between LGE_{DL} and LGE_{O} images was good based on the various SD and FWHM methods (for objective measurements: all ICCs > 0.60, all $P < 0.05$; for P_{area}: all ICCs > 0.70, $P < 0.05$). These measurements were better for LGE_{DL} images than for LGE_{O} images (Figs. 4 and 5).

Analysis and comparison of diagnostic efficacy

All SD methods exhibited good diagnostic efficacy for UMI, with AUC values of the ROC curves ≥ 0.78. The

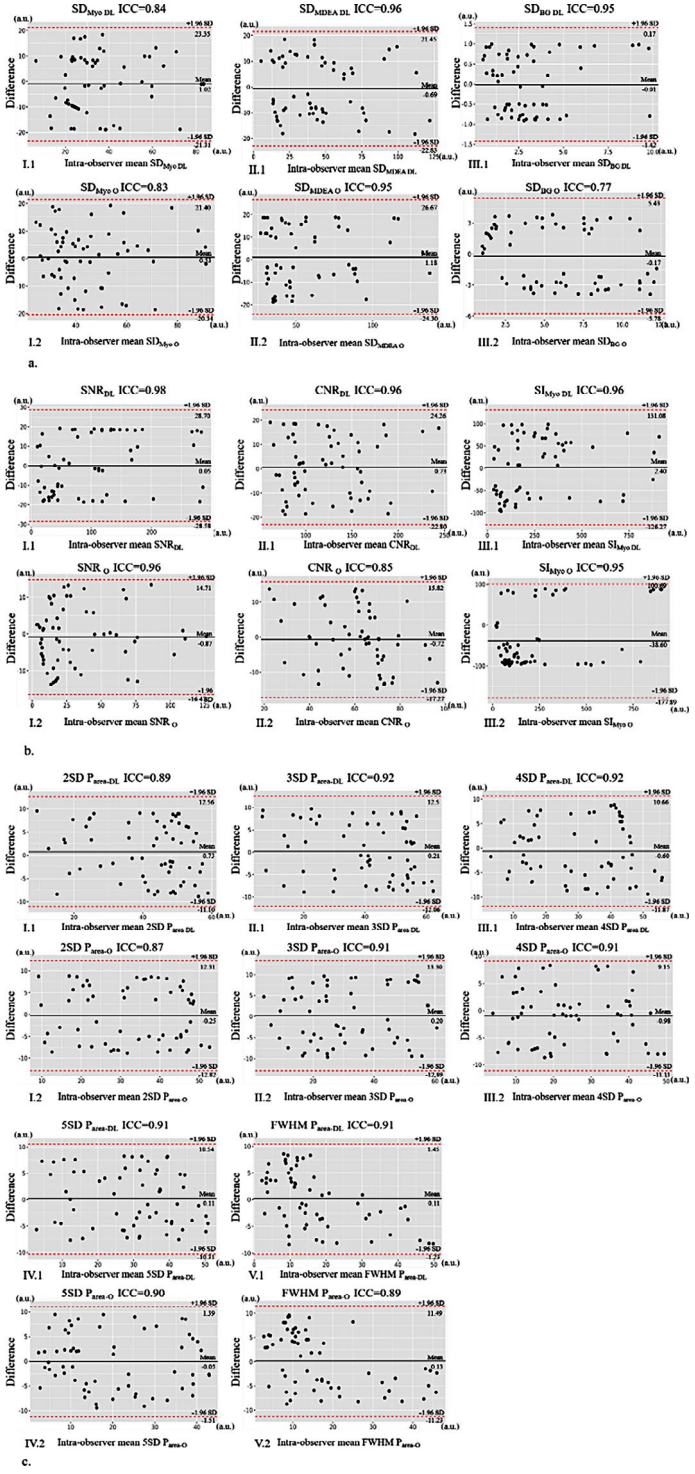

Fig. 4 Bland–Altman plots for the intra-observer (a) SD of myocardium, enhancement area, and background noise; (b) SNR, CNR, SIMyo; (c) 2SD, 3SD, 4SD, 5SD, FWHM; 95% confidence intervals are labelled. There is a very good interstudy agreement for SD and FWHM methods. (1) LGE_{DL} images, (2) LGE_{O} images. Note: DL, deep learning late gadolinium enhancement; O: original late gadolinium enhancement; SD_{Myo}: standard deviation of normal myocardium; SD_{MDEA}: standard deviation of myocardial delayed enhanced area; SD_{BG}: standard deviation of noise at the corner (background) of images; SNR: signal-to-noise ratio; CNR: contrast-to-noise ratio; SI_{Myo}: signal intensity of normal myocardium; P_{area}: percentage of myocardial enhancement area; 2, 3, 4, and 5SD threshold methods: mean P_{area} respectively adding 2, 3, 4, and 5 times of standard deviation of P_{area} as the threshold for myocardial enhancement area; FWHM: full width at half maximum; LGE_{DL}: deep learning-based reconstruction late gadolinium enhancement; LGE_{O}: conventionally constructed late gadolinium enhancement

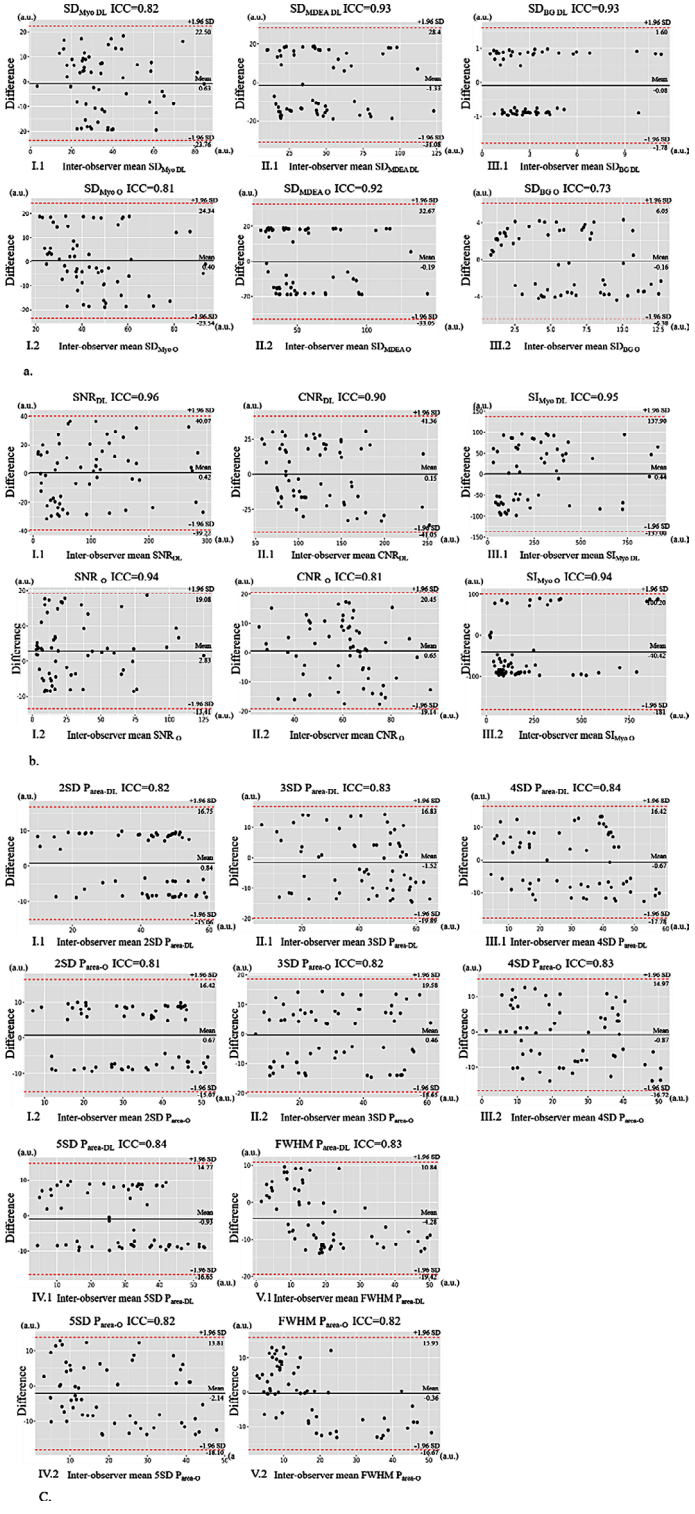

Fig. 5 Bland–Altman plots for the inter- observer analysis; (a) SD of myocardium, enhancement area, and background noise; (b) SNR, CNR, SIMyo; (c) 2SD, 3SD, 4SD, 5SD, FWHM; 95% confidence intervals are labelled. There is a very good interstudy agreement for SD and FWHM methods. (1) LGE_{DL} images, (2) LGE_{O} images. Note: DL: deep learning late gadolinium enhancement; O: original late gadolinium enhancement; SD_{Myo}: standard deviation of normal myocardium; SD_{MDEA}: standard deviation of myocardial delayed enhanced area; SD_{BG}: standard deviation of noise at the corner (background) of images; SNR: signal-to-noise ratio; CNR: contrast-to-noise ratio; SI_{Myo}: signal intensity of normal myocardium; P_{area}: percentage of myocardial enhancement area; 2, 3, 4, and 5SD threshold methods: mean P_{area} respectively adding 2, 3, 4, and 5 times of standard deviation of P_{area} as the threshold for myocardial enhancement area; FWHM: full width at half maximum; LGE_{DL}: deep learning-based reconstruction late gadolinium enhancement; LGE_{O}: conventionally constructed late gadolinium enhancement

Table 3 Area under the curve (AUC) for differentiation of UMI or non-UMI groups

P_{area}	Area	Standard error	*P*	Approaching 95% confidence interval	
				Lower limit	Upper limit
2SD $P_{area-DL}$	0.859	0.066	< 0.05	0.730	0.988
2SD P_{area-O}	0.824	0.073	< 0.05	0.681	0.967
3SD $P_{area-DL}$	0.887	0.057	< 0.05	0.775	0.998
3SD P_{area-O}	0.840	0.069	< 0.05	0.705	0.975
4SD $P_{area-DL}$	0.855	0.066	< 0.05	0.725	0.986
4SD P_{area-O}	0.781	0.084	< 0.05	0.616	0.947
5SD $P_{area-DL}$	0.891	0.056	< 0.05	0.781	0.999
5SD P_{area-O}	0.781	0.085	< 0.05	0.615	0.947
FWHM $P_{area-DL}$	0.797	0.079	< 0.05	0.642	0.951
FWHM P_{area-O}	0.797	0.079	< 0.05	0.643	0.951

Note: SD, standard deviation; $P_{area-DL}$, percentage of myocardial enhancement area with deep learning late gadolinium enhancement; P_{area-O}, percentage of myocardial enhancement area with original late gadolinium enhancement; 2, 3, 4, and 5SD threshold methods, mean P_{area} respectively adding 2, 3, 4, and 5 times of standard deviation of P_{area} as the threshold for myocardial enhancement area; FWHM, full width at half maximum

$P_{area-DL}$ based on the 5SD threshold method exhibited the optimal diagnostic efficacy of 0.891 (sensitivity = 0.688 and specificity = 1). For the conventional imaging enhancement, the P_{area-O} based on the 3SD method exhibited the optimal diagnostic efficacy of 0.840. The diagnostic efficacy was better for LGE_{DL} images than for LGE_O images for UMI detection for every SD threshold method, whereas it was not different between LGE_{DL} and LGE_O parameters based on the FWHM method (Table 3; Fig. 6).

Discussion

This study compared LGE_O and LGE_{DL} images based on different SD thresholds and the FWHM method. The significant differences in P_{area} values between LGE_O and LGE_{DL} images for the SD threshold methods but not for the FWHM method suggested that the STRM should be ≥3, regardless of whether conventional or DLR-based LGE images are used, as previously reported. An STRM≥4 and $P_{area-DL}$ values based on the 5SD threshold exhibited the highest diagnostic efficacy for detecting UMI. Additionally, the LGE_{DL} images generated in this study could display the delayed enhancement area in patients with UMI for the first time, with significantly better image quality than was previously achievable with LGE_O images, such as artifacts in the myocardium, intensified foci and lower background noise, lower SD, and higher SNR and CNR values in all patients with UMI. Thus, LGE_{DL} imaging can improve diagnostic confidence without impacting diagnostic efficacy.

The presence of an infarction in patients with UMI is a critical feature for predicting adverse cardiac events [26–28]. The P_{area} on LGE images is the most frequently used direct indicator of irreversible damage at the pathological tissue level and can predict the treatment response to cardioprotective interventions [29, 30]. However, the clinical approach for quantifying the myocardial enhancement area is not uniform, with SD thresholds used in some instances and the FWHM method employed in others. Additionally, the generation of LGE images using conventional reconstruction and DLR-based methods is inconsistent. Generally, an STRM≥3SD is the optimal reference threshold for clinical use. Quantifying the SD thresholds depends predominantly on the SI and SD of the ROIs drawn in the distal normal myocardium; however, the image quality of the remote normal myocardium may affect the visual sketching of the area to avoid the delayed lesion intensification on LGE_{DL} images [31]. For example, using a lower SD threshold of the distal myocardium leads to a significantly lower threshold for encompassing the extent of delayed enhancement, resulting in underestimation [13]. The SD values, including SD_{Myo}, SD_{MDEA}, and SD_{BG} of the LGE_{DL} images, showed

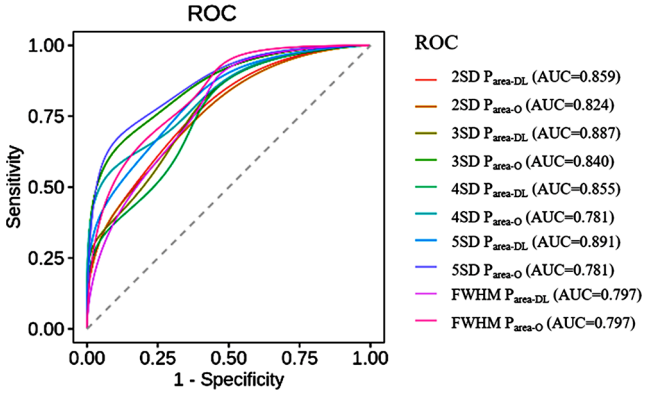

Fig. 6 Diagnostic efficacy for UMI. Note: UMI: unrecognised myocardial infarction; SD: standard deviation; $P_{area-DL}$, percentage of myocardial enhancement area with deep learning late gadolinium enhancement; P_{area-O}, percentage of myocardial enhancement area with original late gadolinium enhancement; 2, 3, 4, and 5SD threshold methods, mean P_{area} respectively adding 2, 3, 4, and 5 times of standard deviation of P_{area} as the threshold for myocardial enhancement area; FWHM: full width at half maximum

similar patterns and were smaller than those of the LGE_O images, consistent with a previous DLR liver study [25]. Higher SNR and CNR values on LGE_{DL} images than on LGE_O images corresponded to improved inter- and intra-reader consistency of P_{area} measurements, indicating a more precise outline of the endocardium, epicardium, and foci boundary in the LGD_{DL} images because of the lower noise levels and fewer motion artifacts, especially in S1 and S16. DL plays a pivotal role in the field of medical image segmentation [17–21]. Currently, manual delineation is subject to certain variabilities. In the future, integrating artificial intelligence-based automatic segmentation optimization may reduce the inconsistencies associated with manual delineation [22, 25–28]. The incremental change in P_{area} values was inconsistent between segments; for example, S12, a middle segment of the lateral wall, exhibited a higher P_{area} on LGE_{DL} images than on LGE_O images, possibly due to less interference from artifacts and clearer edges of the lesion. Regarding the SD methods, the 4SD and 3SD threshold approaches in this study resulted in the highest inter- and intra-reader consistency for $P_{area-DL}$ and the highest intra-reader consistency for P_{area-O}. Therefore, threshold selection for image reconstruction based on conventional and DL-based approaches should be considered cautiously. Consistent with previous findings [12], the $P_{area-DL}$ did not statistically differ from the P_{area-O} values when the FWHM method was used, as the technique only results in noise reduction without altering information fidelity on LGE_{DL} images. It yields highly reproducible and consistent enhanced areas regardless of the underlying etiologies for assessing the severity and extent of MI and other myocardial diseases [13, 16, 26, 32, 33].

This was the first study to evaluate and directly compare LGE_{DL} and LGE_O images of delayed intensification foci in patients with UMI. The diagnostic performance of the $P_{area-DL}$ was higher than that of the P_{area-O} for the threshold approaches, especially for the $P_{area-DL}$ based on the 5SD threshold, which exhibited the best AUC (0.891). For LGE_O images, the P_{area-O} based on the 3SD threshold exhibited the optimal AUC of 0.840, consistent with data from previous studies recommending using an STRM ≥ 3SD for infarct size. This study recruited patients with UMI without clinically significant cardiogenic chest pain and with a relatively small range of reinforcing foci; these results confirm that the 3SD threshold is sufficient for conventional LGE images. In contrast, a threshold ≥ 4SD should be used for DLR LGE images to optimize the intra- and inter-reader agreement and diagnostic efficacy. The diagnosis of the extent of infarction in UMI-related cases using the 4SD threshold was possibly a more reliable parameter for LGE_O and LGE_{DL} images despite the better diagnostic efficacy of the 5SD threshold for LGE_{DL} imaging. Furthermore, the detection rate of UMI was 67% (63/91); this rate was similar for LGE_O and LGE_{DL} images despite the better image quality and more reliable assessment of pathological features on LGE_{DL} imaging.

This study has some limitations. First, all participants were recruited using a single-center design, and only those who underwent an MR examination were included for analysis, limiting the generalizability of our results. Despite LGE images with high diagnostic accuracy of MI detection, the final diagnosis relies on experienced radiologists due to the lack of pathological validation for delayed enhancement areas on LGE images. Therefore, to enhance the robustness of result generalization, multicenter and large data, including comparison of $P_{area-DL}$ and P_{area-O} using various SD and FWHM methods and validation of the accuracy and reliability for UMI diagnosis should be considered for future LGE_O or LGE_{DL}.

Conclusions

The selection of SD thresholds for LGE_{DL} (≥4SD) and LGEO (≥3SD) images was recommended for future research, as the difference between $P_{area-DL}$ and P_{area-O} affected diagnostic efficacy and clinical decision-making in patients with UMI. Moreover, $P_{area-DL}$ and P_{area-O} were similar when the FWHM method was used, implying LGE_{DL} images retained informational integrity. Despite the same UMI detection rates between LGE_O and LGE_{DL} images, the LGE_{DL} images showed superior image quality and reliable features for diagnosis with more confidence. Therefore, STRM selection and diagnostic outcomes should be carefully utilized and interpreted, particularly for DLR-based CMR images.

Abbreviations

MI	Myocardial infarction
UMI	Unrecognized myocardial infarction
DLR	Deep learning reconstruction
SNR	Signal-to-noise ratio
CNR	Contrast-to-noise ratio
P_{area}	Percentage of enhanced area
STRM	Signal threshold versus reference mean
SD	Standard deviation
FWHM	Full width at half maximum
CMR	Cardiac magnetic resonance
LGE_O	Conventionally constructed late gadolinium enhancement
LGE_{DL}	Deep learning-based reconstruction late gadolinium enhancement
MRI	Magnetic resonance imaging
DL	Deep learning
cTn	Cardiac troponin
ROI	Region of interest
SI	Signal intensity
ICC	Intraclass correlation coefficients
ROC	Receiver operating characteristic
AUC	Area under the curve

Supplementary Information

The online version contains supplementary material available at https://doi.org/10.1186/s12880-024-01308-2.

Supplementary Material 1

Acknowledgements
Our thanks are due to the whole team. In addition, thanks are due to Xiaomin Feng, Jing Xie for various useful suggestions and information collection.

Author contributions
XL conceptualization, methodology, data curation, software, experiments, formal analysis, writing – original draft，review and editing of this study. WL conceptualization, methodology, data curation, Formal analysis, Writing – original draft, review and editing of this study. YY experiments, data curation, validation, visualization of this study. WY investigation, methodology, resources, software of this study. CL investigation, methodology, software of this study. WG experiments, data curation, validation of this study. GQ resources, software of this study. JJ data curation, formal analysis of this study. LY data curation, formal analysis of this study. YZ conceptualization of this study, methodology, funding acquisition, data curation, Software, project administration, resources, supervision, writing – review and editing of this study. All authors read and approved the final manuscript.

Funding
This study was supported by the National Natural Science Foundation of China (Grant Numbers 82171895) and the Interdisciplinary Innovative Talents Foundation from Renmin Hospital of Wuhan University (JCRCZN-2022-013).

Data availability
The datasets generated or analyzed during the study are available from the corresponding author on reasonable request.

Declarations

Ethics approval and consent to participate
This study conformed with the tenets of the Declaration of Helsinki and was approved by the institutional review board of Renmin Hospital of Wuhan University Clinical Research Ethics Committee (Approval No. 2022 K-K083). All patients provided written informed consent for study inclusion before magnetic resonance scanning.

Consent for publication
Not applicable.

Competing interests
The authors declare no competing interests.

Author details
[1]Department of Radiology, Renmin Hospital of Wuhan University, No. 238 Jiefang Road, Wuchang District, Wuhan 430060, China
[2]MR Research, GE Healthcare, Beijing, China
[3]GE Healthcare, Beijing, China
[4]Computer School, Wuhan University, Wuhan, China
[5]Information Center, Renmin Hospital of Wuhan University, Wuhan, China

Received: 4 January 2024 / Accepted: 27 May 2024
Published online: 31 May 2024

References

1. Thygesen K, Alpert JS, Jaffe AS, Chaitman BR, Bax JJ, Morrow DA, White HD. Fourth universal definition of myocardial infarction (2018). Circulation. 2018;138:e618–51.
2. Weir-McCall JR, Fitzgerald K, Papagiorcopulo CJ, Gandy SJ, Lambert M, Belch JJF, Cavin I, Littleford R, Macfarlane JA, Matthew SZ, Nicholas RS, Struthers AD, Sullivan FM, Waugh SA, White RD, Houston JG. Prevalence of unrecognized myocardial infarction in a low–intermediate risk asymptomatic cohort and its relation to systemic atherosclerosis, Eur. Heart J Cardiovasc Imaging. 2017;18:657–62.
3. Sugiyama T, Kanaji Y, Hoshino M, Hada M, Misawa T, Nagamine T, Teng Y, Matsuda K, Sayama K, Araki M, Usui E, Murai T, Lee T, Yonetsu T, Sasano T, Kakuta T. Relationship between unrecognized myocardial infarction and underlying coronary plaque characteristics on Optical Coherence Tomography. JACC Cardiovasc Imaging. 2022;15:1830–2.
4. Dastidar AG, Baritussio A, Garate ED, Drobni Z, Biglino1 G, Singhal P, Milano EG, Angelini GD, Dorman S, Strange J, Johnson T. Bucciarelli-Ducci, prognostic role of CMR and conventional risk factors in myocardial infarction with non-obstructed coronary arteries. JACC Cardiovasc Imaging. 2019;12:1973–82.
5. Pesapane F, Codari M, Sardanelli F. Artificial intelligence in medical imaging: threat or opportunity? Radiologists again at the forefront of innovation in medicine. Eur Radiol Exp. 2018;2:35.
6. Kim C, Park CH, Kim DY, Cha J, Lee BY, Park CH, Kang EJ, Koo HJ, Kitagawa K, Cha MJ, Krittayaphong R, Choi SI, Viswamitra S, Ko SM, Kim SM, Hwang SH, Trang NN, Lee W, Kim YJ, Lee J, Yang DH. Semi-quantitative scoring of late Gadolinium Enhancement of the left ventricle in patients with ischemic cardiomyopathy: improving Interobserver Reliability and Agreement using Consensus Guidance from the Asian Society of Cardiovascular Imaging-Practical Tutorial (ASCI-PT). Eur Heart J Cardiovasc Imaging. 2022;23:298–307.
7. Cha MJ, Kim SM, Kim Y, Kim HS, Cho SJ, Sung J, Choe YH. Unrecognized myocardial infarction detected on cardiac magnetic resonance imaging: Association with coronary artery calcium score and cardiovascular risk prediction scores in asymptomatic Asian cohort. PLoS ONE. 2018;13:e0204040.
8. Kodai Sayama M, Hoshino Y, Kanaji T, Sugiyama T, Misawa M, Hada T, Nagamine K, Nogami. Yun Teng, Hiroki Ueno, Kazuki Matsuda, Taishi Yonetsu, Tsunekazu Kakuta. Prognostic implications of non-infarct-related territory unrecognized myocardial infarction in patients with non-ST-segment-elevation acute coronary syndrome. J Cardiol. 2023;82:433–40.
9. Théo Pezel T, Unterseeh M, Kinnel T, Hovasse F, Sanguineti. Solenn Toupin3, Stéphane Champagne, Philippe Garot1 and Jérôme Garot. Long-term prognostic value of stress perfusion cardiovascular magnetic resonance in patients without known coronary artery disease. J Cardiovasc Magn Reson. 2021; 23.
10. Hoshino M, Sugiyama T, Kanaji Y, Hada M, Nagamine T, Nogami K, Ueno H, Sayama K, Matsuda K. Taishi Yonetsu, Tetsuo Sasano, Tsunekazu Kakuta. Multimodality coronary imaging to predict non-culprit territory unrecognized myocardial infarction in Non-ST-Elevation acute coronary syndrome. Int J Cardiovasc Imaging. 2023;39:2051–61.
11. Demirkiran A, Everaars H, Amier RP, Beijnink C, Bom MJ, Götte MJW, van Loon RB, Selder JL, van Rossum AC, Nijveldt R. Cardiovascular magnetic resonance techniques for tissue characterization after acute myocardial injury. Eur Heart J Cardiovasc Imaging. 2019;20:723–34.
12. Pradella S, Mazzoni LN, Letteriello M, Tortoli P, Bettarini S, De Amicis C, et al. FLORA software: semi-automatic LGE-CMR analysis tool for cardiac lesions identification and characterization. Radiol Med. 2022;127:589–601.
13. van der Velde N, Hassing HC, Bakker BJ, Wielopolski PA, Lebel RM, Janich MA, et al. Improvement of late gadolinium enhancement image quality using a deep learning–based reconstruction algorithm and its influence on myocardial scar quantification. Eur Radiol. 2021;31:3846–55.
14. Flett AS, Hasleton J, Cook C, Hausenloy D, Quarta G, Ariti C, et al. Evaluation of techniques for the quantification of myocardial scar of differing etiology using cardiac magnetic resonance. JACC Cardiovasc Imaging. 2011;4:150–6.
15. Zucker EJ, Sandino CM, Kino A, Lai P, Vasanawala SS. Free-breathing accelerated Cardiac MRI using deep learning: validation in children and young adults. Radiology. 2021;300:539–48.
16. Giuseppe Muscogiuri C, Martini M, Gatti, et al. Feasibility of late gadolinium enhancement (LGE) in ischemic cardiomyopathy using 2D-multisegment LGE combined with artificial intelligence reconstruction deep learning noise reduction algorithm. Int J Cardiol. 2021;343:164–70.
17. Shambhu S, Koundal D, Das P, Sharma C. Binary classification of COVID-19 CT images using CNN: COVID diagnosis using CT. Int J E Health Med Commun. 2021;13:1–13.
18. Shambhu S, Koundal D, Das P. Deep learning-based computer assisted detection techniques for malaria parasite using blood smear images. Int J Adv Technol Eng Explor. 2023;10:990–1015.
19. Shambhu S, Koundal D, Das P. Edge-based segmentation for accurate detection of malaria parasites in microscopic blood smear images: a novel approach using FCM and MPP algorithms, 2023 2nd International Conference on Smart Technologies and Systems for Next Generation Computing (ICSTSN), Villupuram, India, 2023, pp. 1–6.
20. Shambhu S, Koundal D. Recent trends in image processing using granular computing. Lecture Notes Electr Eng. 2020;668.

21. Shambhu S, Koundal D, Das P, Hoang VT, Tran-Trung K, Turabieh H. Computational methods for automated analysis of malaria parasite using blood smear images: recent advances. Comput Intell Neurosci. 2022; 3626726.
22. Barbier CE, Themudo R, Bjerner T, Johansson L, Lind L, Ahlström H. Long-term prognosis of unrecognized myocardial infarction detected with cardiovascular magnetic resonance in an elderly population. J Cardiovasc Magn Reson. 2016;18:43–9.
23. Cheong BY, Duran C, Preventza OA, Muthupillai R, Muthupillai. Comparison of low-dose higher-relaxivity and standard-dose lower-relaxivity contrast media for delayed-enhancement MRI: a blinded randomized crossover study. Am J Roentgenol. 2015;205:533–9.
24. Andrew S, Flett J, Hasleton C, Cook, et al. Evaluation of techniques for the quantification of myocardial scar of differing etiology using cardiac magnetic resonance, JACC. Cardiovasc Imaging. 2011;4:150–6.
25. Chen Q, Fang S, Yuchen Y, Li R, Deng R, Chen Y, Ma D. Huimin Lin, Fuhua Yan. Clinical feasibility of deep learning reconstruction in liver diffusion-weighted imaging: improvement of image quality and impact on apparent diffusion coefficient value. Eur J Radiol. 2023.
26. Ganesan AN, Gunton J, Nucifora G, McGavigan AD, Selvanayagam JB. Impact of late gadolinium enhancement on mortality, sudden death and major adverse cardiovascular events in ischemic and nonischemic cardiomyopathy: a systematic review and meta-analysis. Int J Cardiol. 2018;254:230–7.
27. Halliday BP, Baksi AJ, Gulati A, Ali A, Newsome S, Izgi C, Arzanauskaite M, Lota A, Tayal U, Vassiliou VS, Gregson J, Alpendurada F, Frenneaux MP, Cook SA, Cleland JGF, Pennell DJ, Prasad SK. Outcome in dilated cardiomyopathy related to the extent, location, and pattern of late gadolinium enhancement. JACC Cardiovasc Imaging. 2019;12:1645–55.
28. Weng Z, Yao J, Chan RH, He J, Yang X, Zhou Y, Yang H. Prognostic value of LGE CMR in HCM: a meta-analysis. JACC Cardiovasc Imaging. 2016;9:1392–402.
29. Stone GW, Selker HP, Thiele H, Patel MR, Udelson JE, Ohman EM, Maehara A, Eitel I, Granger CB, Jenkins PL, Nichols M, Ben-Yehuda O. Relationship between infarct size and outcomes following primary PCI: patient-level analysis from 10 randomized trials. J Am Coll Cardiol. 2016;67:1674–83.
30. Taylor AM. The role of artificial intelligence in paediatric cardiovascular magnetic resonance imaging. Pediatr Radiol. 2021;22:1–8.
31. Bustin A, Janich MA, Brau AC, Odille F, Wolff SD, Shubayev O, Stanley D, Menini A. Joint denoising and motion correction: initial application in single-shot cardiac MRI. J Cardiovasc Magn Reson. 2015;17:Q29.
32. Mikami Y, Kolman L, Joncas SX, Stirrat J, Scholl D, Rajchl M, Lydell CP, Weeks SG, Howarth AG, White JA. Accuracy and reproducibility of semi-automated late gadolinium enhancement quantification techniques in patients with hypertrophic cardiomyopathy. J Cardiovasc Magn Reson. 2014;16:85–94.
33. Antiochos P, Ge Y, Steel K, Bingham S, Abdullah S, Mikolich JR, Arai AE, Bandettini WP, Patel AR, Farzaneh-Far A, Heitner JF, Shenoy C, Leung SW, Gonzalez JA, Shah DJ, Raman SV, Ferrari VA, Schulz-Menger J, Stuber M, Simonetti OP, Kwong RY. SPINS study investigators, imaging of clinically unrecognized myocardial fibrosis in patients with suspected coronary artery disease. J Am Coll Cardiol. 2020;76:945–57.

Publisher's Note